Si−E (E = N, O, F) Bonding in a Hexacoordinated Silicon Complex: New Facts from Experimental and Theoretical Charge Density Studies

Nikolaus Kocher,[†] Julian Henn,[‡] Boris Gostevskii,[§] Daniel Kost,[§] Inna Kalikhman,[§] Bernd Engels,[‡] and Dietmar Stalke*,[†]

Contribution from the Institut für Anorganische und Organische Chemie, Universität Würzburg, Am Hubland, 97074 Würzburg, Germany, and Department of Chemistry, Ben-Gurion University of the Negev, Beer-Sheva 84105, Israel

Received September 11, 2003; E-mail: dstalke@chemie.uni-wuerzburg.de

Abstract: The concept of hypervalency in molecules, which hold more than eight valence electrons at the central atom, still is a topic of constant debate. There is general interest in silicon compounds with more than four substituents at the central silicon atom. The dispute, whether this silicon is hypervalent or highly coordinated, is enlightened by the first experimental charge density determination and subsequent topological analysis of three different highly polar Si−E (E = N, O, F) bonds in a hexacoordinated compound. The experiment reveals predominantly ionic bonding and much less covalent contribution than commonly anticipated. For comparison gas-phase ab initio calculations were performed on this compound. The results of the theoretical calculations underline the findings of the experiment.

1. Introduction

The concept of hypervalency in molecules, which hold more than eight valence electrons at the central atom, still is a topic of constant debate.[1] Especially for compounds with strongly electron-withdrawing substituents, it seems that this concept is not useful; e.g., recent studies proved that sulfur imides and phosphonium ylides should not be described as hypervalent species with S=N and P=C bonds.[2,3] Since the past decades there is general interest in silicon compounds with more than four substituents at the central silicon atom.[4] The dispute of whether this silicon is hypervalent or highly coordinated is a paradigmatic case in which the presence or absence of a bond is believed to be deducible from merely geometrical features extracted from routine structure determinations.[5] However, topological analysis of the experimentally determined charge density of these bonds provides a much more powerful tool for

elucidating the nature of the bonding far beyond bond lengths and angles considerations.

As early as 1939, Pauling, on the basis of ΔEN between Si and O, came to the conclusion that a Si−O bond has about 50% covalent character rather than being purely ionic;[6] nevertheless the nature of the Si−O bond still remains controversial.[7] However, studies are mainly focused on silicates. To the best of our knowledge, topological studies on Si−N bonds as well as those on Si−F bonds based on data from high-resolution X-ray experiments are not yet available.[8]

In this paper we provide the first topological analysis of a hexacoordinated silicon atom in an organosilicon compound. Difluorobis[*N*-(dimethylamino)phenylacetimidato-*N*,*O*]silicon (**1**; Figure 1) is a convenient example as it contains three different sets of highly polar silicon−element bonds (Si−E, E = N, O, F) in the same molecule.[9] The classification of the Si−E bonds is based on various criteria deduced from the results of a multipole refinement based on high-resolution X-ray data: electron density, the Laplacian along the bond path, and its spatial distribution around the electronegative atoms. Furthermore, we calculated the total electronic energy density and the kinetic energy density at the bond critical point (BCP) and obtained experimental charges from the integration over the

  [†] Institut für Anorganische Chemie, Universität Würzburg.
  [‡] Institut für Organische Chemie, Universität Würzburg.
  [§] Ben-Gurion University of the Negev.
 (1) (a) Kutzelnigg, W. *Angew. Chem.* **1984**, *96*, 202; *Angew. Chem., Int. Ed.* **1984**, *23*, 272. (b) Gillespie, R. J.; Silvie, B. *Coord. Chem. Rev.* **2002**, *233*, 53.
 (2) (a) Leusser, D.; Walfort, B.; Stalke, D. *Angew. Chem.* **2002**, *114*, 2183; *Angew. Chem., Int. Ed.* **2002**, *41*, 2079. (b) Leusser, D.; Henn, J.; Kocher, N.; Engels, B.; Stalke, D. *J. Am. Chem. Soc.* **2004**, *126*, 1781.
 (3) (a) Gilheany, D. G. *Chem. Rev.* **1994**, *94*, 1339. (b) Dobado, J. A.; Martinez-Garcia, H. M.; Molina J. M.; Sundberg M. R. *J. Am. Chem. Soc.* **2000**, *122*, 1144.
 (4) (a) Kost, D.; Kalikhman, I. In *Chemistry of Organosilicon Compounds*; Wiley: Chichester, U.K., 1998. (b) Kost, D.; Kingston, V.; Gostevskii, B.; Ellern, A.; Stalke, D.; Walfort, B.; Kalikhman, I. *Organometallics* **2002**, *21*, 2293. (c) Kost, D.; Gostevskii, B.; Kocher, N.; Stalke, D.; Kalikhman, I. *Angew. Chem.* **2003**, *115*, 1053; *Angew. Chem., Int. Ed.* **2003**, *42*, 1023.
 (5) (a) Chuit C.; Corriu, R. J. P.; Reye, C.; Young, J. C. *Chem. Rev.* **1993**, *93*, 1371. (b) Schiemenz, G. P.; Schiemenz, B.; Petersen, S.; Wolff, C. *Chirality* **1998**, *10*, 180.

 (6) Pauling, L. *The Nature of the Chemical Bond*; Cornell University Press: Ithaca, NY, 1939.
 (7) Gibbs, G. V.; Downs, J. W.; Boisen, M. B., Jr. *Rev. Mineral.* **1994**, *29*, 331.
 (8) (a) Theoretical study of a Si−N bond: Wang, J.; Eriksson, L. A.; Boyd, R. J.; Shi Z. *J. Phys. Chem.* **1994**, *98*, 1844. (b) Experimental charge density distribution in K_2SiF_6 but without quantitative topological analysis: Herster, J. R.; Maslen, E. N. *Acta Crystallogr.* **1995**, *B51*, 913.
 (9) Routine crystal structure from standard diffraction experiment to $2\theta_{max} = 53°$ (Mo Kα) published in: Kalikhman, I.; Gostevskii, B.; Girshberg, O.; Sivaramakrishna, A.; Kocher, N.; Stalke, D.; Kost, D. *J. Organomet. Chem.* **2003**, *686*, 202.
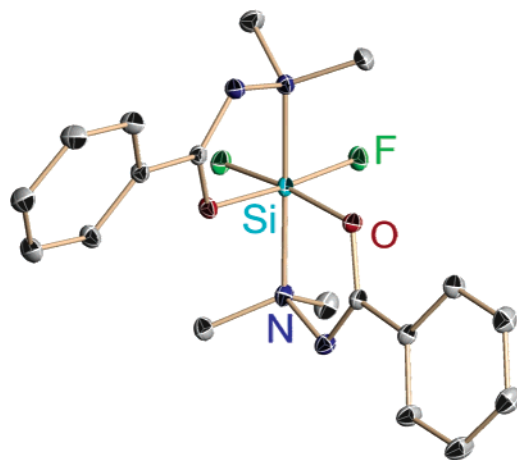
Figure 1. Solid-state structure of **1**. Hydrogen atoms are omitted for clarity. The asymmetric unit contains only half of the molecule. The second part is generated by a 2-fold axis at the bisection of the O−Si−O angle, the silicon atom is located on a special position. Anisotropic displacement parameters are depicted at the 50% probability level.

atomic basins. The properties at the BCP as well as the Laplacian distribution, the above-mentioned energies, and the atomic charges are compared to the results derived from theoretical calculations.

2. Experimental Conditions and Refinement

A well-shaped, oil-coated crystal, obtained from cooled diethyl ether solution, was mounted on a glass fiber. The diffraction experiment was performed up to a scattering angle of $2\theta_{max} = 108.6°$ ($\sin (\theta/\lambda) = 1.14$ Å^{-1}; $d = 0.43$ Å) and an overall completeness of approximately 98% within 5 days.[10] Data were collected on a Bruker APEX-CCD diffractometer (graphite-monochromated Mo Kα radiation, $\lambda = 0.710\ 73$ Å) equipped with a low-temperature device at 100(2) K[11] in Ω-scan mode with only two different detector positions ($2\theta = 31$ and 80°, respectively). For integration and data reduction the programs SAINT,[12] SORTAV,[13] and XPREP[14] were applied, respectively.

In multipole refinement 11 448 unique reflections were employed ($\sin (\theta/\lambda_{max}) = 1.10$ Å^{-1}) according to the Hansen and Coppens formalism,[15] which is implemented in the full-matrix least-squares refinement program (XDLSM) of the XD program package[16] up to the hexadecapole level using statistical weights $w_H = 1/\sigma_H^2$ during the refinement. The final difference Fourier map is featureless and the results of the rigid-bond test reveal that the electron density is properly deconvoluted from thermal motion, although the mass differences in the Si−E bonds are not neglectable.[17] From the obtained multipole parameters,[18] a topological analysis of the charge density was performed

and atomic properties were evaluated using new features in XDPROP,[16] TOPXD,[19] and WinXPRO.[20] Further details of the experiment and the refinement are available in the Supporting Information.

3. Theoretical Details

The gas-phase structure of **1** was optimized at the B3LYP/ 6-311G** level of theory, which in a previous study showed converged density properties.[2b] In all calculations C_2 symmetry was imposed. Stationary points of this calculation were checked by frequency calculations. The difference in total energy of the experimentally determined solid-state geometry, which was used as a starting point for the optimization and the fully optimized geometry at this level of theory, is smaller than 4 kcal/mol. All optimized geometries from density functional theory (DFT) calculations remain very close to the experimental geometry. The only apparent effect is the relaxing of the slightly twisted phenyl group into a coplanar geometry with the N2−C3−O1 plane. All calculations were performed with the Gaussian98 package.[21a] The subsequent topological analyses were performed with the AIM2000 package.[22] The NBO/NRT analyses were performed with the NBO 4.0 package employing the B3LYP/ 6-311G** level of theory.[21b]

4. Results and Discussion

The theory of "atoms in molecules" (AIM)[23] allows for judgment the nature of chemical interactions based on experimental electron densities rather than being limited to the indirect classification based on the comparison of connectivities and geometrical features of routine structure determinations. To characterize the Si−E bonds, we have analyzed $\rho(\mathbf{r})$ and the Laplacian $\nabla^2\rho(\mathbf{r})$ in terms of Bader's theory of AIM. We found all anticipated BCPs in the bonding regions. They are located closely to the electropositive silicon atom (see Table 1 and Figure 2). However, the displacement from the center of the bond path is more pronounced for the Si−F and the Si−O bond in the theoretical results. The consequences of these altering positions are different topological values from experimental and theoretical studies at the BCP. This is a well-known problem in combined experimental and theoretical studies.[24,25] Nevertheless, the relatively good agreement of experiment and theory can be deduced from the topological properties at the BCP of

(10) Crystallographic data for refinement of high-resolution data set: Monoclinic; space group, *C2/c*; *a* = 19.844(2) Å, *b* = 8.537(2) Å, *c* = 12.068(2) Å; *β* = 113.7310(10)°; *V* = 1871.51(11) Å³; *Z* = 4; *μ* = 0.166 mm⁻¹; 53 909 reflections measured, 11 448 unique; *R*(int) = 0.0537 (low angles) and 0.0738 (high angles); wR2 (all data) = 0.1052; R1 (*I* > 4σ(*I*)) = 0.0420, for 126 parameters. Crystallographic data have been deposited with the Cambridge Crystallographic Data Centre as supplementary publication no. CCDC-208970.
(11) Kottke, T.; Stalke, D. *J. Appl. Crystallogr.* **1993**, *26*, 615. (b) Kottke, T.; Lagow, R. J.; Stalke, D. *J. Appl. Crystallogr.* **1996**, *29*, 465. (c) Stalke, D. *Chem. Soc. Rev.* **1998**, *27*, 171.
(12) *SAINT: Area-Detector Integration Software*; Bruker-AXS Inc.: Madison, WI, 1995.
(13) Implemented in WINGX: Farrugia, L. J. *J. Appl. Crystallogr.* **1999**, *32*, 837. Using the algorithm of: Blessing, B. *Acta Crystallogr.* **1995**, *A51*, 33.
(14) XPREP implemented in: *SHELXTL*; Bruker-AXS Inc.: Madison, WI, 2000.
(15) Hansen, N. K.; Coppens, P. *Acta Crystallogr.* **1978**, *A34*, 909.
(16) Koritsanszky, T.; Howard, S.; Richter, T.; Su, Z. W.; Mallinson, P. R.; Hansen, N. K. *XD—A Computer Program Package for Multipole Refinement and Analysis of Electron Densities from Diffraction Data. User Manual*; Freie Universität: Berlin, Germany, 1995.
(17) Hirshfeld, F. L. *Acta Crystallogr.* **1976**, *A32*, 239.

(18) For further details see Supporting Information.
(19) Volkov, A.; Gatti, C.; Abramov, Y. A. *Acta Crystallogr.* **2000**, *A56*, 252.
(20) Stash, A.; Tsirelson. V. WinXPRO: A Program for Calculating Crystal and Molecular Properties Using Multipole Parameters of the Electron Density. *J. Appl. Crystallogr.* **2002** *35*, 371.
(21) (a) Frisch, M. J.; Trucks, G. W.; Schlegel, H. B.; Scuseria, G. E.; Robb, M. A.; Cheeseman, J. R.; Zakrzewski, V. G.; Montgomery, J. A., Jr.; Stratmann, R. E.; Burant, J. C.; Dapprich, S.; Millam, J. M.; Daniels, A. D.; Kudin, K. N.; Strain, M. C.; Farkas, O.; Tomasi, J.; Barone, V.; Cossi, M.; Cammi, R.; Mennucci, B.; Pomelli, C.; Adamo, C.; Clifford, S.; Ochterski, J.; Petersson, G. A.; Ayala, P. Y.; Cui, Q.; Morokuma, K.; Malick, D. K.; Rabuck, A. D.; Raghavachari, K.; Foresman, J. B.; Cioslowski, J.; Ortiz, J. V.; Baboul, A. G.; Stefanov, B. B.; Liu, G.; Liashenko, A.; Piskorz, P.; Komaromi, I.; Gomperts, R.; Martin, R. L.; Fox, D. J.; Keith, T.; Al-Laham, M. A.; Peng, C. Y.; Nanayakkara, A.; Gonzalez, C.; Challacombe, M.; Gill, P. M. W.; Johnson, B.; Chen, W.; Wong, M. W.; Andres, J. L.; Gonzalez, C.; Head-Gordon, M.; Replogle, E. S.; Pople, J. A. *Gaussian 98*, revision A.7; Gaussian, Inc.: Pittsburgh, PA, 1998. (b) Glendening, E. D.; Badenhoop, J. K.; Reed, A. E.; Carpenter, J. E.; Weinhold, F. *NBO 4.M*; Theoretical Chemistry Institute, University of Wisconsin: Madison, WI, 1999.
(22) Biegler-König, F.; Schonbohm, J.; Bayles, D. AIM2000—A Program to Analyze and Visualize Atoms in Molecules. *J. Comput. Chem.* **2001**, *22*, 545.
(23) Bader, R. F. W. *Atoms in Molecules—A Quantum Theory*; Clarendon Press: Oxford, U.K., 1990.
(24) Bach, A.; Lentz, D.; Luger, P. *J. Phys. Chem.* **2001**, *A105*, 7405.
(25) Volkov, A.; Abramov, Y.; Coppens, P.; Gatti, C. *Acta Crystallogr.* **2000**, *A56*, 332.

Table 1. Topology of the Si–E (E = N, O, F) Bonds in **1**[a]

A–B	d(A–B)	d(A–BCP)	d(BCP–B)	$\rho(r_{BCP})$	$\nabla^2\rho(r_{BCP})$	$H(r_{BCP})$	$G(r_{BCP})/\rho(r_{BCP})$	$|\lambda_1|/\lambda_3$	charge (B)[b]
Si–F	1.6397	0.7040	0.9357	1.015(13)	13.472(33)	−0.076	1.43	0.26	−0.80
	(1.6673)	(0.6923)	(0.9750)	(0.769)	(18.200)	(−0.039)	(1.78)	(0.17)	(−0.85)0
Si–O	1.7789	0.7476	1.0313	0.766(13)	7.373(29)	−0.052	1.14	0.29	−1.21
	(1.7975)	(0.7209)	(1.0766)	(0.6643)	(10.905)	(−0.048)	(1.38)	(0.20)	(−1.29)
Si–N	1.9703	0.7627	1.2076	0.501(16)	7.755(32)	−0.011	1.23	0.20	−0.78
	(1.9998)	(0.7679)	(1.2319)	(0.565)	(4.385)	(−0.049)	(0.91)	(0.27)	(−0.85)

[a] In each column the upper entry denotes experimental values, and the lower entry in brackets gives theoretical values from B3LYP/6-311G** calculations: $d(A–B)$, distance between atoms A and B along the bond path in Å; $d(A–BCP)$, $d(BCP–B)$, distances between BCP and atoms A and B, respectively; $\rho(r_{BCP})$, charge density at the BCP in e Å^{-3}; $\nabla^2\rho(r_{BCP})$, Laplacian of $\rho(r)$ at the BCP in e Å^{-5}. Electronic energy density $H(r_{BCP})$ is in atomic units (au); charges from the integration over the atomic basin, in electrons (e). [b] Charge of Si (A in A–B) = +2.78 e (+3.13 e).
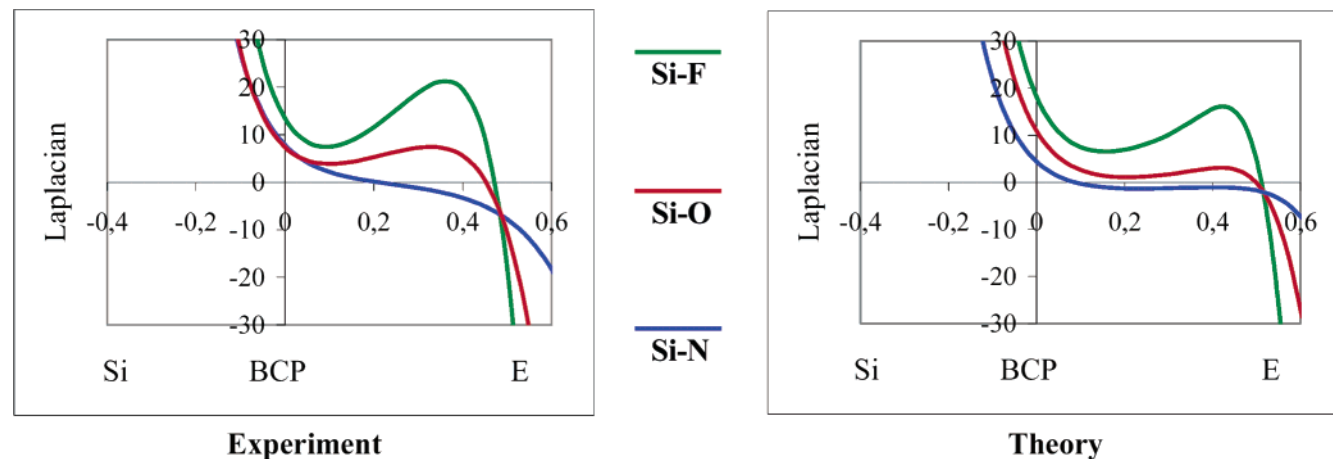
Figure 2. Experimental and theoretical Laplacians along the Si–E (E = F, O, N) bond paths.

the Si–E bonds. The positions of the experimental and theoretical BCPs in **1** differ only marginally. Furthermore, the spatial distribution of properties such as the Laplacian is also important in comparative studies.[2b] The values of the total density $\rho(r)$ and the Laplacian at the BCP in the phenyl ring[18] of **1** match those of other compounds,[26] further supporting the credibility of the used model. A ring critical point could be determined in the center of the phenyl rings as well as in the SiOCN$_2$ five-membered heterocycles, respectively.

The Si–O as well as the Si–F bond lengths from experiment are in the range normally observed for hexacoordinated silicon compounds.[4] The electron density at the BCP of the Si–E bonds derived from the experiment is remarkably low compared to those bonds classified as polar covalent bonds, including third row elements such as S and P.[2,26] The density of 0.5 e Å^{-3} at the BCP of the dative Si–N bond (196.61(3) pm) is extremely low. This is only half the amount found for shorter Si–N bonds (e.g., in [c-Me$_2$SiN(H)]$_4$, d_{av} = 172.5(5) pm).[27] Apart from the distance, this value hints toward the different bonding situation along the Si–N vector in **1**.

The Laplacian, the algebraic sum of the three principal curvatures λ_1, λ_2, and λ_3 of $\rho(r)$, is the appropriate tool for localizing and characterizing regions of local charge concentration and depletion. The nature of the atomic interaction depends on the dominant curvatures. Shared interactions (covalent bonds) are dominated by the negative curvatures (λ_1, λ_2); charge is

concentrated in the internuclear region. This charge concentration is reflected by a large value of $\rho(r)$ and by a negative value of the Laplacian $\nabla^2\rho(r)$. For closed-shell interactions (ionic bonds), the positive curvature λ_3 is dominant; charge is depleted at the BCPs as a result of the contraction of $\rho(r)$ toward each nucleus, and the spatial distribution of the Laplacian is predominately atom-like. This charge depletion is characterized by a low value of $\rho(r)$ and by a positive value of $\nabla^2\rho(r)$.[28] The Laplacian distribution of the atoms bonded to silicon, depicted in Figure 3, shows an almost spherical distribution around O and F, almost identical for experiment and theory. The spatial distribution of the Laplacian in the N1–Si–N1A plane depicts small differences. The deformation of the lone-pair toward the silicon atom is more pronounced in the Laplacian distribution of the theoretical results, caused by a more significant charge transfer from the silicon to the nitrogen atom. This is in tune with the more prominent charge differences in the AIM model from theory (Δ_{charge}(Si,N), 3.98 e) compared to the experiment (3.56 e). Both deformations of the lone-pair charge concentration around the nitrogen atom indicate polarization toward the silicon atom. This polarization can directly be scaled to the electronegativities: the lower the EN is, the more the deformation is pronounced. While it is significant with the nitrogen atom (Figure 3b,d), it is only marginally with the oxygen atoms, and with the fluorine atoms it is virtually not detected. Figure 3 visualizes this gradual decay both in the experiment but even more emphasized in theory. In a detailed study of dative bonds, based on theoretical data, Jonas et al. demonstrated that all dative N→E′ (E′ = B, Al) bonds with characteristic deformations of the charge concentrations toward the acceptor atom revealed

(26) Yuffit, D. S.; Howard, J. A. K.; Davidson, M. G. *J. Chem. Soc., Perkin Trans. 2* **2000**, 249.

(27) Topological properties of the Si–N bonds in 1,1,2,2,3,3,4,4-octamethyl-cyclotetrasilazane [c-Me$_2$Si–N(H)]$_4$ after multipole refinement (preliminary values, averaged over all Si–N bonds of the molecule, are presented): $\rho(r_{BCP})$ = 0.987(56) e Å^{-3}; $\nabla^2\rho(r_{BCP})$ = 8.1136(566) e Å^{-5}; distance of N atoms from BCP, 0.9984(53) Å; distance of Si atoms from BCP, 0.7270-(49) Å. Kocher, N.; Stalke, D. To be published.

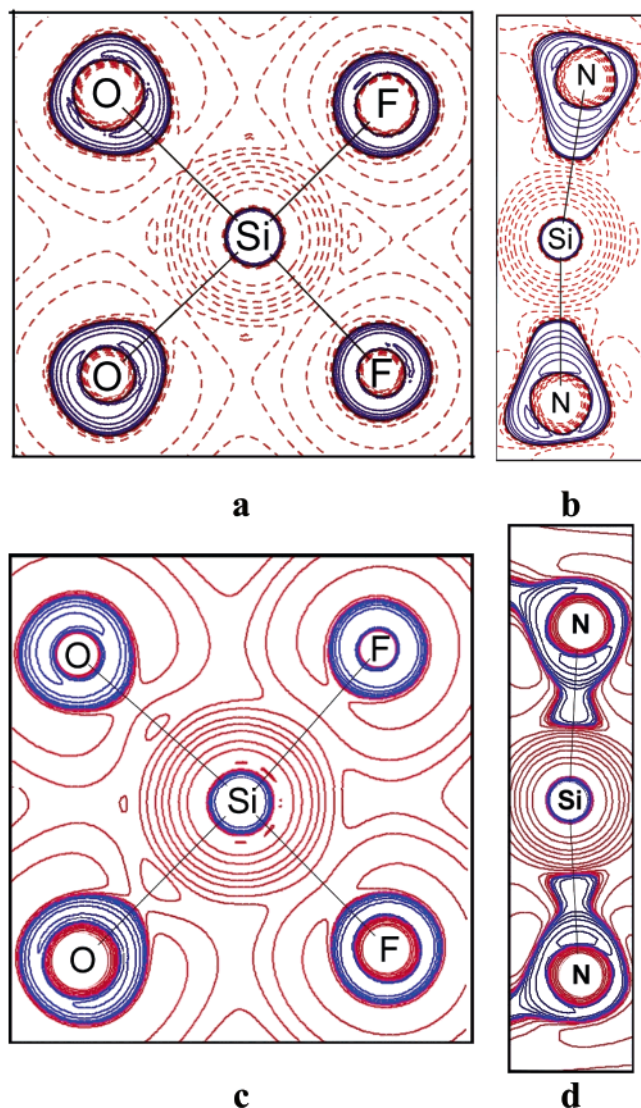(28) Koritsanszky, T. S.; Coppens, P. *Chem. Rev.* **2001**, *101*, 1568.

a

b

c

d

Figure 3. Laplacian in the O_2SiF_2 plane. Not all atoms are exactly in this plane (a, experiment; c, theory) and the SiN_2 plane (b, experiment; d, theory) of **1**; positive values of $\nabla^2\rho(\mathbf{r})$ are depicted by red and negative by blue lines. Contours drawn at 0.000, $\pm 2.0 \times 10^n$, $\pm 4.0 \times 10^n$, and $\pm 8.0 \times 10^n$ e Å^{-5}, where $n = 0, \pm 1, \pm 2, \pm 3$.

significant covalent contribution.[29] In the present study we examine if this argumentation is applicable to the Si−E bonds in **1**.

As the position of the BCP is vital and the values differ with slight variations of the position, we decided to monitor the Laplacian along the whole bond path.[30] The Laplacians at the BCPs for the three different Si−E bonds are all positive with the maximum at the Si−F bond of $\nabla^2\rho(\mathbf{r}_{BCP}) = 13.472$ followed by the Si−N and Si−O bond with 7.755 and 7.373 e Å^{-5}, respectively.

From Figure 2 it is obvious that the Laplacian along the three bond paths is positive at any point in the silicon basin, indicating charge depletion in a sphere with a radius considerably larger than the distance Si−BCP. The situation along the Si−F and

Si−O bond path is similar: experiment and theory reveal positive values at the BCP and in the entire bonding region with a more positive Laplacian for the Si−F bond at each point. Close to the more electronegative atom the Laplacian changes rapidly due to charge concentrations. Despite almost the same values at the BCP for the Si−N and Si−O bonds in the experiment, the Si−N bond shows a different Laplacian distribution in the basin of the nitrogen atom. The Laplacian is close to zero in a long range of the bonding region. This distribution of the Laplacian along the Si−N bond is also visible from theoretical results.

Moreover, we carried out intensive searches for $(3;−3)$ critical points in the spatial distribution of $-\nabla^2\rho(\mathbf{r})$ from the experimental and theoretical data to localize and quantify maximum charge concentrations in the bonding and nonbonding regions in the valence shell of an atom; these areas are so-called valence shell charge concentrations (VSCCs). With this procedure we gain information about the Laplacian distribution apart from the bonding regions. Inspection of the VSCCs around the electronegative atoms in the coordination sphere of the Si atom led to interesting results (Figure 4). Around the donating N atom a sharp maximum is located on the bonding vector directed toward the silicon atom. The lone pairs of the fluorine atom tend to couple from two sides toward the silicon bonding vector (Figure 4d) indicating redistribution of charge in the Si−F bond and thus explaining the rather high value of $\rho(\mathbf{r})$ at the BCP for this bond.[31] The banana-shaped VSCC of the oxygen atom encloses the maxima of the lone pair region (Figure 4c); due to the rather diffuse shape of this VSCC, the exact maxima of the expected two lone pairs could not be deconvoluted, neither in the experiment nor in theory.[32] However, the situation around the oxygen atom is special because the bond lengths in addition to the electron density and the Laplacian distributions indicate a slight delocalization of charge toward the neighboring carbon atom. Local concentrations and depletions of the electrons in the internuclear space are connected with the features of the electronic energy distribution via the local form of the virial theorem.[33] It describes an exact relationship between the second derivative of the electron density, $\nabla^2\rho(\mathbf{r})$, the electronic kinetic energy density $(G(\mathbf{r}))$[34] and the electronic potential energy density $(V(\mathbf{r}))$. The total electronic energy density $H(\mathbf{r})$ with $H(\mathbf{r}) = G(\mathbf{r}) + V(\mathbf{r})$[35] provides a straight criterion for the classification of the atomic interaction: $H(\mathbf{r}_{BCP}) < 0$ is observed in shared-type (covalent) atomic interactions, while $H(\mathbf{r}_{BCP}) \geq 0$ is observed in purely closed-shell (ionic) interactions.[29,36,37] Typical values of $H(\mathbf{r}_{BCP})$ for covalent single bonds cluster around -0.35.[36] Moreover, the ratio $G(\mathbf{r}_{BCP})/\rho(\mathbf{r}_{BCP})$ hints to the nature of the interactions between two atoms. The ratio $G(\mathbf{r}_{BCP})/\rho(\mathbf{r}_{BCP})$ should be less than unity for shared interaction (covalent bond) and greater than unity for closed-shell (ionic) interaction. All Si−E bonds in **1** have a total electronic energy density at the BCP close to zero. The electronic energy density

(29) Jonas, V.; Frenking, G.; Reetz, M. T. *J. Am. Chem. Soc.* **1994**, *116*, 8741. Jonas et al. found values of $\rho(r)$ between 0.08 and 0.73 e Å^{-3} for dative bonds with nitrogen donors and positive Laplacians for all of these bonds.
(30) Tafipolsky, M.; Scherer, W.; Oefele, K.; Artus, G.; Pedersen, B.; Herrmann, W. A.; McGrady, G. S. *J. Am. Chem. Soc.* **2002**, *124*, 5865.
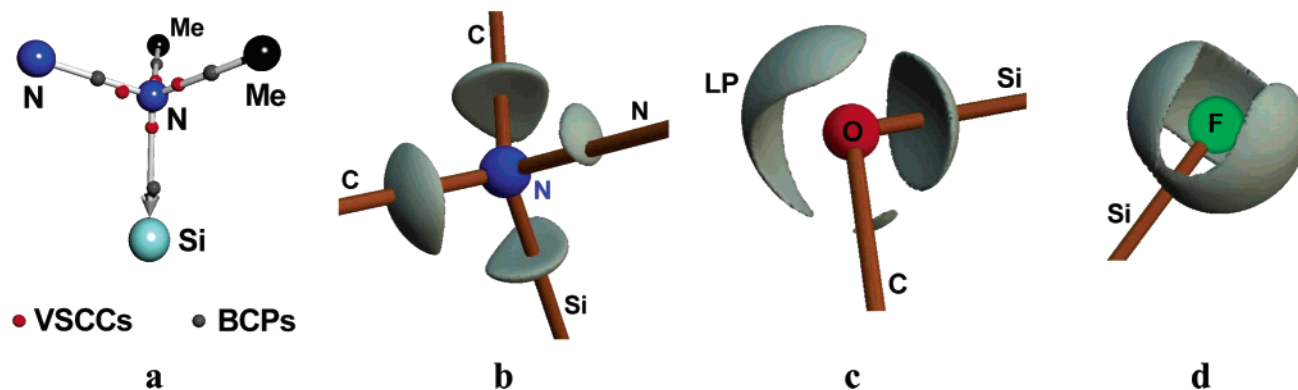
(31) Chesnut, D. B. *Chem. Phys.* **2003**, *291*, 141.
(32) We do not distinguish between nonbonding pairs and lone pairs as suggested by Chesnut.[31] Electron pairs and charge concentrations not located on or close to a bonding vector are named/termed lone pairs and nonbonding charge concentrations, respectively.
(33) Bader, R. F. W.; Beddall, P. M. *J. Chem. Phys.* **1972**, *56*, 3320.
(34) Kirzhnits, D. A. *Sov. Phys.−JEPT* **1957**, *32*, 115.
(35) Bader, R. F. W.; Essen, H. *J. Chem. Phys.* **1984**, *80*, 1943.
(36) Cremer, D.; Kraka, E. *Angew. Chem.* **1984**, *96*, 612; *Angew. Chem., Int. Ed. Engl.* **1984**, *23*, 627.
(37) Bone, R. G. A.; Bader, R. F. W. *J. Phys. Chem.* **1996**, *B100*, 10892.
(38) Abramov, Y. A. *Acta Crystallogr.* **1997**, *A53*, 264.

Figure 4. (a) Critical points around the donating nitrogen atoms. Valence shell charge concentrations (VSCCs) in $\nabla^2\rho(\mathbf{r})$ are marked in red and BCPs in gray, respectively. (b–d) Isosurface maps at constant $-\nabla^2\rho(\mathbf{r})$ values indicating bonding and nonbonding charge concentrations around the displayed atoms: (b) N1, $-\nabla^2\rho(\mathbf{r}) = 48$ e Å^{-5}; (c) O, $-\nabla^2\rho(\mathbf{r}) = 92$ e Å^{-5}; (d) F, $-\nabla^2\rho(\mathbf{r}) = 180$ e Å^{-5}.

of the Si–N bond, derived from experimental data, equals zero, those for Si–F and Si–O are slightly negative. Although the deformation of the charge concentration at the donating nitrogen atom toward the silicon atom suggests at first sight high negative values for $H(\mathbf{r}_{BCP})$ as reported from Jonas et al.,[29] the electronic energy density is practically zero at the BCP of the N→Si bond. For the Si–F and the Si–O bond the energy $H(\mathbf{r}_{BCP})$ is slightly negative, in toto indicating absolutely ionic domination in the Si–N bond and predominantly ionic character with small covalent contributions for Si–F and Si–O (Table 1). The theoretical $H(\mathbf{r}_{BCP})$ values are more alike for the three different bonds. Those of the Si–O and the Si–F bonds are less negative compared to experimental values, the electronic energy density of the Si–N bond is slightly more negative, also leading to ionic domination for all three Si–E bonds. The values for the ratio $G(\mathbf{r}_{BCP})/\rho(\mathbf{r}_{BCP})$ are all above or close to unity. The Si–F bond shows the highest ratio in the experimental and theoretical model.

The ratio of $|\lambda_1|/\lambda_3$ at the BCP is an additional tool to classify a bond.[39] For ionic bonds (closed-shell interaction) this quotient should be below 1 because of the large value of λ_3; in addition the values for λ_1 and λ_2 are small compared to those in a bond with shared interaction. Values of 0.26 (0.17), 0.29 (0.20), and 0.20 (0.27) (theoretical values in brackets) for the Si–F, Si–O, and Si←N bonds, respectively, affirm the findings in the Laplacian. From the experimental data the ratio for the dative Si←N bond underlines most the domination of λ_3 at the BCP and thus a local charge depletion. In contrast, the results from theory assign the lowest ratio to the Si–F bond.

A reliable atomic charge can be derived from the integration of the electron density over the atomic basin. These basins are the result of a partitioning of a molecule into atomic regions with boundaries according to Bader's AIM theory. The integrations of the atomic basins result in a highly positive silicon atom and negative charges for fluorine, oxygen, and nitrogen, respectively (Table 1). The AIM charges from theory are marginally more negative for each atom E (E = N, O, F). Therefore the charge of the atom in the center of these six atoms is even more positive. The atomic basins (from experiment) of the SiOCN$_2$ heterocycle are displayed in Figure 5. Also from the NBO calculation a considerable positive charge at the silicon atom can be deduced (Si, +2.27; N, −0.43; O, −0.81; F, −0.66
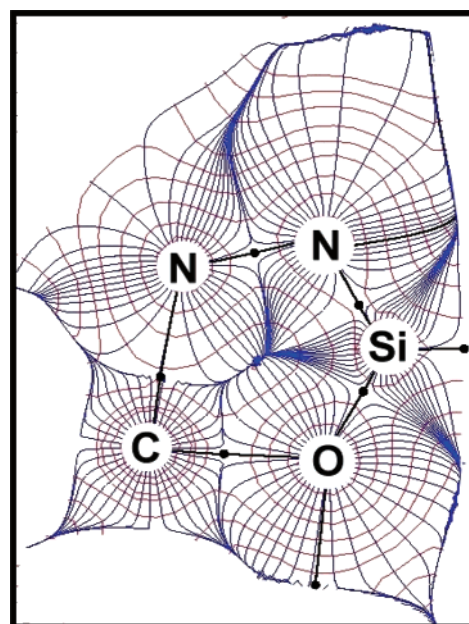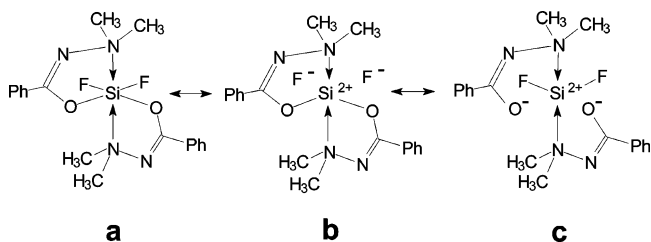
(39) Coppens, P. *X-ray Charge Densities and Chemical Bonding*; Oxford University Press: Oxford, U.K., and New York, NY, 1997.

Figure 5. Two-dimensional trajectory plot in a plane of the SiOCN$_2$ heterocycle, visualizing the different shapes and sizes of the atomic basins. Red lines denote electron density, and blue lines are trajectories of the electron density; bond paths and BCPs are black.

Scheme 1. Lewis Structures for **1** (Theoretical Charges in Electrons from NBO Analysis: Si, +2.27; N, −0.43; O, −0.81; F, −0.66 e)

e). The NBO charge of higher than +2 unequivocally proves that the canonical forms **b** and **c** depicted in Scheme 1 contribute most to explain the bonding in **1**.

5. Conclusion

Considering all electronic features determined from the analyses of experimental and theoretical data, we conclude that the silicon atom in **1** definitely is not hypervalent. Two different

kinds of bonds around the hexacoordinated center are present. The Si−N bonds in **1** clearly are dative bonds with completely different properties than shorter nondative Si−N bonds. The question of whether dative bonds are to be classified as covalent or ionic remains controversial. However, almost all properties in **1**, derived from both experiment and theory, suggest ionic domination, and it is just the deformation of the lone pair charge concentration that might introduce a notable covalent contribution. The four remaining Si−E (E = O, F) bonds indicate predominantly ionic contributions and just a small covalent augmentation. The slightly negative electronic energy density and the amount of electron density at the BCP support covalent contributions, while the positive Laplacian in the entire bonding region, an atomic like Laplacian distribution; the ratio $|\lambda_1|/\lambda_3$ smaller than 0.3 suggests ionic domination. The topological properties at the BCPs of the Si−E bonds as well as the calculated energy densities and the AIM charges derived from experiment and theory are in very good agreement. The consistence of the Laplacian distribution in the planes of the ligands, a property not limited to one single point but visualizing the charge distribution around the central atom, is evident. Both analyses underline the dominating ionic character of these bonds. Together with the NBO charge definitely higher than +2 for the silicon atom all the electronic properties emphasize the dominance of the Lewis structures **b** and **c** in Scheme 1 to the appropriate bond description, and the covalent contribution obviously is much lower than commonly anticipated.

Note Added after ASAP Publication: The Si−N bond distance cited in the text from ref 27 was reported in angstroms, not picometers, in the version published on the Web 4/2/2004. The final version published 4/6/2004 and the print version are correct. Several minor changes to the text were also made.

Supporting Information Available: Experimental section, with crystal data tables for **1**, including atomic coordinates after multipole refinement, local coordinate systems, multipole populations, residual densities bond lengths and angles, anisotropic displacement parameters, bond critical points, critical points in the Laplacian distribution around the nitrogen atoms, and theoretical section, with atomic coordinates of optimized geometry, critical points, eigenvalues. X-ray crystallographic data for **1** (CIF). This material is available free of charge via the Internet at http://pubs.acs.org.

JA038459R